

Intertwined orders of ultracold fermions loaded in two-dimensional optical lattices

A. Leprévost¹, O. Juillet¹ and R. Frésard²

¹ *Laboratoire LPC Caen, ENSICAEN, Université de Caen, CNRS/IN2P3, Caen, France.*

² *Laboratoire CRISMAT, UMR CNRS-ENSICAEN 6508, Caen, France.*

The generic quantum phase diagram of repulsively interacting spin-1/2 ultracold atoms, moving in a two-dimensional optical lattice, is investigated by means of unbiased energy minimizations with symmetry-adapted unrestricted wavefunctions. In the strongly correlated regime, we highlight the intertwining of spin-, charge-, and pair-density waves embedded in a uniform d -wave superfluid background. As the lattice filling increases, this phase emerges from homogenous states exhibiting spiral magnetism and evolves towards a doped antiferromagnet. A concomitant enhancement of long-ranged d -wave pairing correlations is also found. Nevertheless, superfluidity is suppressed when the charge period and the inverse of the hole doping from half-filling are commensurate.

Low dimensional interacting quantum matter generally exhibits several phases at low energy that challenges the ability to distinguish between competing orders and their intertwining within one single correlated state [1]. Ultracold atoms provide an ideal playground to capture the essence of this problematic by their potential to properly emulate the fundamental mechanisms of quantum many-body physics [2]. In the fermionic sector, the BCS-to-BEC crossover [3,4] and the question of Stoner's itinerant ferromagnetism in repulsive gases [5,6] have been investigated. By trapping atomic vapors in optical lattices, a mimic of ideal crystalline matter can also be achieved [7]. By now, direct images of Fermi surfaces in the non-interacting limit [8] as well as s -wave superfluidity near unitary scattering [9] have been reported. Away from a Feshbach resonance, one is able to engineer almost perfectly the celebrated Hubbard model that has been first considered to describe the magnetism of metallic systems [10]. More generally, it aims to grasp the generic properties of spin-1/2 fermions moving on a lattice by hopping between neighboring sites $\langle \vec{r}, \vec{r}' \rangle$ and experiencing a local two-body interaction of strength U . In second-quantized form, the Hamiltonian is given by

$$\hat{H} = -t \sum_{\langle \vec{r}, \vec{r}' \rangle \sigma} \hat{c}_{\vec{r}\sigma}^\dagger \hat{c}_{\vec{r}'\sigma} + U \sum_{\vec{r}} \hat{n}_{\vec{r}\uparrow} \hat{n}_{\vec{r}\downarrow}, \quad (1)$$

with t the hopping integral; The fermionic creation, annihilation and density operators at site \vec{r} with spin label $\sigma \in \{\uparrow, \downarrow\}$ are $\hat{c}_{\vec{r}\sigma}^\dagger$, $\hat{c}_{\vec{r}\sigma}$ and $\hat{n}_{\vec{r}\sigma} = \hat{c}_{\vec{r}\sigma}^\dagger \hat{c}_{\vec{r}\sigma}$, respectively. In the attractive regime, spin-polarized systems could exhibit several exotic superfluid phases [11] while the BCS-to-BEC transition has been addressed in the spin-balanced model [12]. Otherwise, the on-site repulsion can stand for a perfectly screened Coulomb interaction and it received a considerable renewed interest in two-dimensional (2D) geometry after Anderson's proposal [13] in connection to the spectacular properties of the high- T_c cuprates. However, there is still no consensus about the adequacy of the positive- U Hubbard model to capture the interplay between d -wave superconductivity, magnetism and inhomogeneous phases of copper oxides.

This challenging issue is even more relevant since latest condensed-matter experiments seem to be consistent with an intriguing scenario where spin, density and long-ranged pair correlations develop cooperatively and are spatially modulated [14,15].

The exact answer to the question of whether the 2D repulsive Hubbard model supports such intertwining of multiple orders will probably be provided only through quantum emulators like ultracold atoms. Indeed, exact low energy properties of the Hamiltonian Eq. (1) are only accessible in one dimension [16] and for the infinitely connected Bethe lattice through the dynamical mean-field theory [17]. In other cases, computational methods to recover exact ground-states are generally marred by an exponential complexity [18,19]. Nevertheless, diagrammatic quantum Monte-Carlo (QMC) simulations in continuous-time have recently allowed for a determination of the phase diagram at weak coupling for small to intermediate filling [20]. Even if ultracold fermions in optical lattices already enabled to monitor the Mott transition [21] and the development of antiferromagnetic correlations at half-filling [22], the knowledge of the phase diagram at low temperature and up to the strongly repulsive limit remains a long-term goal. In spirit of the compelling example provided by unitary Fermi gases [23], it is highly desirable to introduce theoretical approximate schemes that could guide experiments and benefit from the progressive results of this emulation.

In order to embrace the full complexity of the repulsive 2D Hubbard model, we set up in this Letter a variational scheme with totally unrestricted wavefunctions and demonstrate for the hole doped regime the intertwining of magnetic, density and pairing channels in the quantum phase diagram. Correlations beyond mean-field are generated by restoring deliberately broken symmetries through quantum number projection. In fact, the Hamiltonian Eq. (1) is invariant under local $U(1)$ gauge transformations, lattice translations, spin rotations and discrete symmetries of the lattice. Thus, exact eigenstates are characterized by the number of fermions N , the total pseudo-momentum \vec{K} , the total spin S and its z -component S_z , as well as an irreducible representation of the lattice symmetry group. All these labels will be collectively denoted by Γ in the following. Their restoration on top of a single Hartree-Fock (HF) wavefunction and before energy minimization recently yielded encouraging results for 2D clusters [24]. In particular, the exact ground-state of the four-site model has been recovered irrespective of the interaction strength [25]. The approach, and its analog with several Slater determinants [26,27], also proved capable to evidence interplay between spin, charge and pair degrees of freedom. Potential superfluid features would nevertheless require a very large number of HF basis states to be accurately captured, whereas Bogoliubov-de Gennes (BdG) ansätze are well known to be more appropriate. Hence, we focus on a more entangled trial state $|\Psi_\Gamma\rangle$ obtained through the coherent superposition of symmetry projected HF and BdG wavefunctions:

$$|\Psi_\Gamma\rangle = \hat{P}_\Gamma \left(x^{(HF)} |\Phi^{(HF)}\rangle + x^{(BdG)} |\Phi^{(BdG)}\rangle \right) \quad (2)$$

Here, $|\Phi^{(HF)}\rangle = \prod_{i=1}^N \hat{c}_{\phi_i}^\dagger | \rangle$ with $\hat{c}_{\phi_i}^\dagger = \sum_{\vec{r}\sigma} \phi_{i,\vec{r}\sigma} \hat{c}_{\vec{r}\sigma}^\dagger$ denoting the most general Slater determinant, and $|\Phi^{(BdG)}\rangle \propto \prod_{\vec{r}\sigma} \hat{\gamma}_{\vec{r}\sigma} | \rangle$ with $\hat{\gamma}_{\vec{r}\sigma} = \sum_{\vec{r}'\sigma'} V_{\vec{r}'\sigma',\vec{r}\sigma}^* \hat{c}_{\vec{r}'\sigma'}^\dagger + U_{\vec{r}'\sigma',\vec{r}\sigma}^* \hat{c}_{\vec{r}'\sigma'}$ the most general quasi-particle

vacuum. The operator \hat{P}_Γ ensures the projection on quantum numbers Γ and, according to group theory, may be expressed as a specific linear combination of symmetry transformations. Thus, the variational ansatz Eq. (2) appears as a superposition of numerous symmetry-related

mean-field states. Stationarity of the projected energy $E_\Gamma = \langle \hat{H} \rangle_{\Psi_\Gamma}$ with respect to the amplitudes $x^{(HF)}$, $x^{(BdG)}$, the spin-orbitals $\phi_{i,\vec{r}\sigma}$ and the Bogoliubov coefficients $U_{\vec{r}'\sigma',\vec{r}\sigma}$, $V_{\vec{r}'\sigma',\vec{r}\sigma}$ leads to a system of self-consistent equations [28] that allows to determine the optimal HF/BdG symmetry-projected states Eq. (2) without any initial assumption. The numerical solution of this scheme shows an excellent agreement with exact results in the magnetic, density and pairing channels. Several representative cases are detailed in the Supplemental Material [28]. For 4×4 hole-doped clusters, the ground-state energy is also accurately reproduced with a maximum 0.5% relative error for large couplings U/t . As the size of the cell grows, extending the approach with the superposition of several HF/BdG wavefunctions notably improves the energy. For instance, for $N = 56$ interacting atoms on a 16×4 cell at $U/t = 12$, E_Γ is lowered from $-34.413 t$ to $-36.018 t$ with ten HF/BdG pairs. Note that a subspace twice as large is required to reach a similar energy without BdG wavefunctions [27]. Nevertheless, no significant change in the spin, charge and pairing correlation functions has been found during this extension of the trial variational subspace.

In order to unravel the relevant orders and their potential intertwining contained in the above described variational states, we first address the hole doping $\delta \approx 16\%$ from half-filling in the strongly interacting regime $U/t = 12$ which could be appropriate for superconducting cuprates. We consider $N = 54$ atoms on a rectangular 16×4 cell with antiperiodic boundary conditions in the x -direction and periodic ones along the y -axis. Such a configuration enables long wavelength modes and can indicate the emergence of an off-diagonal long-ranged order linked with superfluidity [29]. We present on Fig. 1 the magnetic $S_m(\vec{q})$ and density $S_c(\vec{q})$ structure factors resulting from energy minimization with the symmetry-projected ansatz Eq. (2):

$$S_m(\vec{q}) = \frac{4}{3} \sum_{\vec{R}} \exp(i\vec{q} \cdot \vec{r}) \langle \hat{S}_0 \cdot \hat{S}_{\vec{r}} \rangle_{\Psi_\Gamma}, \quad S_c(\vec{q}) = \sum_{\vec{R}} \exp(i\vec{q} \cdot \vec{r}) \langle \delta \hat{n}_0 \delta \hat{n}_{\vec{r}} \rangle_{\Psi_\Gamma} \quad (3)$$

where $\hat{S}_{\vec{r}} = \frac{1}{2} \sum_{\sigma,\sigma'} \hat{c}_{\vec{r}\sigma}^+ \vec{\tau}_{\sigma,\sigma'} \hat{c}_{\vec{r}\sigma'}$ is the spin operator at lattice node \vec{r} (with $\vec{\tau}$ the usual Pauli matrices) and $\delta \hat{n}_{\vec{r}} = \sum_{\sigma} (\hat{n}_{\vec{r}\sigma} - \langle \hat{n}_{\vec{r}\sigma} \rangle_{\Psi_\Gamma})$ the local charge fluctuation. A coexistence of spin and charge density waves is clearly evidenced by a peak in S_m and S_c on top of a broad background. The dominant wavevector $\vec{q}_m = (3\pi/4, \pi)$ in the spin-spin correlations corresponds to an antiferromagnet with a staggered magnetization oscillating in amplitude with a period of $\lambda_m = 8$ lattice spacings in the x -direction. Similarly, the density-density correlation function reveals inhomogeneities distributed with a period $\lambda_c = 4$ along the x -axis in the variational ground-state. Note that these orders and their symmetry-related counterparts are necessarily superimposed to respect all invariances of the Hamiltonian. Furthermore, the relation $\lambda_m = 2\lambda_c$ characterizes stripes at the boundaries of antiferromagnetic domains separated by a π phase shift. Their intertwining with d -wave superfluidity is eventually proved by highlighting in Fig.2b a non-zero average of the pairing correlation function $\mathcal{D}(\vec{R})$ at large separation distance r . $\mathcal{D}(\vec{r})$ is obtained as:

$$\mathcal{D}(\vec{r}) = \frac{1}{2} \langle \hat{D}_0^\dagger \hat{D}_{\vec{r}} + \hat{D}_0 \hat{D}_{\vec{r}}^\dagger \rangle \quad (4)$$

with $\hat{D}_{\vec{r}}^\dagger = \sum_{\vec{l}} f(\vec{l}) \frac{1}{\sqrt{2}} (\hat{c}_{\vec{r}\uparrow}^\dagger \hat{c}_{\vec{r}+\vec{l}\downarrow}^\dagger - \hat{c}_{\vec{r}\downarrow}^\dagger \hat{c}_{\vec{r}+\vec{l}\uparrow}^\dagger)$ the singlet pair-field in the $d_{x^2-y^2}$ channel where the form factor $f(\vec{l}) = +1$ is zero except for neighboring sites in the x - and y -direction: $f(\pm\vec{u}_x) = 1$ and $f(\pm\vec{u}_y) = -1$ [30]. The non-decaying tail observed for $r > 4$ is consistent with off-diagonal long-ranged order that signs superfluidity. Besides, the 4-period small oscillations of $\mathcal{D}(\vec{r})$ around its averaged value indicate the existence of pairs at a finite momentum equal to the charge-order wavevector. Such stripes with a d -wave superfluidity spatially modulated in phase with the density profile have also been proposed in recent simulations [31,32] of the t - J Hamiltonian that approximates the Hubbard model in the limit $U/t \rightarrow \infty$.

We now address the evolution of the intertwining between spin, charge and pair degrees of freedom with doping at strong coupling $U/t = 12$. Stripe-like states are robust against a decrease of the hole number as shown in Fig. 1 for the 16×4 cluster considered here. However, the shift of the peaks in the structure factors S_m and S_c reflects a doubling of the period when crossing $\delta = 1/8$. In addition, pairing correlations at large distance are totally suppressed in the 8 and 4 hole systems corresponding to perfectly filled and half-filled 8-period vertical stripes, respectively (see Fig. 2c). This spin and charge pattern is also realized for $N = 58$, which now induces doped antiferromagnetic domains allowing a revival of the d -wave superfluid signal. As for $N = 54$, the inverse doping is not commensurate with the charge period and again the behavior of $\mathcal{D}(\vec{r})$ at large distance is consistent with the development of a pair-density wave of period λ_c . When moving towards the half-filling limit, antiferromagnetism no longer exhibits amplitude modulation and a uniform density profile is recovered. Finally, a pure d -wave off-diagonal long-ranged order is unambiguously supported as long as such a background is doped with few holes (see Fig. 2b for $N = 62$). Another scenario emerges when considering an increase of the hole doping from $\delta \approx 16\%$. While peaks related to charge-density waves disappear, incommensurate spin-spin correlations persist with a crossover from horizontal to diagonal order. They could either correspond to collinear spins or to spirals [33]. One way to test whether spins rotate on the lattice is to detect a non-decaying four-body correlation function between spin chirality vectors $\hat{V}_{\vec{r}} = \hat{S}_{\vec{r}} \wedge (\hat{S}_{\vec{r}+\vec{u}_x} + \hat{S}_{\vec{r}+\vec{u}_y})$ as a function of separation distance. The calculation of $\mathcal{V}(\vec{r}) = \langle \hat{V}_0 \cdot \hat{V}_{\vec{r}} \rangle_{\Psi_T}$ at $U = 12t$ for different densities is shown in Fig. 3. The long-ranged ($r > 4$) part systematically displays an oscillating behavior reflecting significant quantum fluctuations. Two regimes are however clearly distinguished: Spiral correlations averaged over large distances vanish in striped and antiferromagnetic states ($N \geq 54$), while they are non-zero and positive at larger dopings. This signal remains of small amplitude and thus rather characterizes a spiral ordering component embedded in a spin-density wave (SDW). The d -wave pairing correlation function in such a state displays a complex behavior at large distance, yet free of a rapid decay to zero as was found at half-filling or in the stripes at commensurate dopings. It can be viewed as the precursor of the d -wave superfluidity that is better established for larger lattice fillings.

The unbiased energy minimization with the symmetry projected HF/BdG wavefunction essentially exhibits all the above features from the intermediate coupling

$U/t=6$ to the strongly correlated regime $U/t=12$. The results are summarized in the quantum phase diagram shown in Fig. 4 for hole doping δ smaller than $1/4$. Stripe-like states are stabilized in the intermediate doping range and once U/t exceeds a critical value. The latter is suppressed with decreasing δ , in agreement with inhomogeneous dynamical mean-field [34] and constrained-path QMC approaches [35]. In addition, the change of the charge period from $\lambda_c = 4$ to $\lambda_c = 8$ takes place when crossing $\delta = 1/8$ and for $U \geq 10t$. Close to the half-filling limit, only antiferromagnetic correlations persist, while stripes melt for larger doping. Instead, incommensurate antiferromagnetism in the form of coexisting spiral and spin-density waves is found. It develops along the x -direction for intermediate interaction strengths ($6 \leq U/t \leq 8$) and tends towards the diagonal direction at large U/t . Furthermore, the spiral component appears for couplings that increase with the doping. Finally, long-ranged d -wave pairing correlations are systematically evidenced, except when all the holes are perfectly trapped into filled or half-filled vertical stripes. These trends are altered at smaller U/t . In particular, for $U/t=4$, charge inhomogeneities are missing and a clear tendency towards magnetic ordering is obtained for dopings smaller than $\delta < 16\%$ only, in agreement with latest diagrammatic QMC calculations [20]. Eventually, the superfluid signal is rather erratic, though this non-monotonicity proved stable against changes of boundary conditions to investigate the influence of shell effects, commonly invoked at small coupling in the attractive regime [36].

Summarizing, we have highlighted insights into generic features of repulsively interacting ultracold fermions loaded in 2D optical lattices through their description by the Hubbard model. The since long proposed scenario of d -wave superfluidity emerging from a doped Mott insulator has been put forward through unrestricted energy minimizations. Nevertheless, such intertwining of magnetic and pair degrees of freedom manifests itself under various facets depending on whether antiferromagnetic correlations grow from homogenous collinear spins, spatially modulated spin-density waves or spirals. It also involves the charge degree of freedom as stripes that either destroy or support superfluidity according to the commensurability between the charge period and $1/\delta$. These features have been extracted from unbiased symmetry-adapted states originating from quantum number projection that also induces correlations beyond mean-field. Furthermore, magnetic, charge and superfluid correlations remain robust against improvements of this wavefunction. The quantum phase diagram therefore provides an additional reference for the cross-validation between theory and quantum emulation from experiments that is necessary to face the exponential complexity of low dimensional quantum matter.

This research was partly supported by the ANR through the GeCoDo project (ANR-11-JS08-001-01). We are grateful to the Région Basse-Normandie and the Ministère de la Recherche for financial support.

- [1] E. Fradkin and S.A. Kivelson, *Nature Phys.* **8**, 865 (2012).
- [2] I. Bloch, J. Dalibard and W. Zwerger, *Rev. Mod. Phys.* **80**, 885 (2008).
- [3] M. W. Zwierlein, J. R. Abo-Shaer, A. Schirotzek, C. H. Schunck and W. Ketterle, *Nature* **435**, 1047 (2005).
- [4] M. W. Zwierlein, C. H. Schunck, A. Schirotzek and W. Ketterle, *Nature* **442**, 54 (2006).
- [5] C. Sanner, E. J. Su, W. Huang, A. Keshet, J. Gillen and W. Ketterle, *Phys. Rev. Lett.* **108**, 240404 (2012).
- [6] G.-B. Jo, Y.-R. Lee, J. H. Choi, C. A. Christensen, T. H. Kim, J. H. Thywissen, D. E. Pritchard and W. Ketterle, *Science* **325**, 1521 (2009).
- [7] M. Lewenstein, A. Sampera, V. Ahufinger, B. Damski, A. Sen De and U. Sen, *Adv. Phys.* **56**, 243 (2007).
- [8] M. Köhl, H. Moritz, T. Stöferle, K. Günter and T. Esslinger, *Phys. Rev. Lett.* **94**, 080403 (2005).
- [9] J. K. Chin, D. E. Miller, Y. Liu, C. Stan, W. Setiawan, C. Sanner, K. Xu and W. Ketterle, *Nature* **443**, 961 (2006).
- [10] J. Hubbard, *Proc. Roy. Soc. London A* **276**, 238 (1963).
- [11] Y. L. Loh and N. Trivedi, *Phys. Rev. Lett.* **104**, 165302 (2010).
- [12] A. Sewer, X. Zotos and H. Beck, *Phys. Rev. B* **66**, 14504(R) (2002).
- [13] P.W. Anderson, *Science* **235**, 1196 (1987).
- [14] Z. Xu, C. Stock, S. Chi, A.I. Kolesnikov, G. Xu, G. Gu and J. M. Tranquada, *Phys. Rev. Lett.* **113**, 177002 (2014).
- [15] E. Fradkin, S. A. Kivelson and J. M. Tranquada, arxiv:1407.4480 (2014).
- [16] E. H. Lieb and F.Y. Wu, *Phys. Rev. Lett.* **20**, 1445 (1968).
- [17] R. Bulla, A. C. Hewson, and Th. Pruschke, *J. Phys.: Condens. Matter* **10**, 8365 (1998).
- [18] M. Troyer and U.-J. Wiese, *Phys. Rev. Lett.* **94**, 170201 (2005).
- [19] S. Liang and H. Pang, *Phys. Rev. B* **49**, 9214 (1994).
- [20] Y. Deng, E. Kozik, N. Prokof'ev and B. Svistunov, arXiv:1408.2088 (2014).
- [21] R. Jördens, N. Strohmaier, K. Günter, H. Moritz and T. Esslinger, *Nature* **455**, 204 (2008).
- [22] R. A. Hart, P. M. Duarte, T.-L. Yang, X. Liu, T. Paiva, E. Khatami, R. T. Scalettar, N. Trivedi, D. A. Huse and R. G. Hulet, Advance online publication, *Nature* (2015).
- [23] K. Van Houcke, F. Werner, E. Kozik, N. Prokof'ev, B. Svistunov, M. J. H. Ku, A. T. Sommer, L. W. Cheuk, A. Schirotzek, M. Zierlein, *Nature Phys.* **8**, 366 (2012).
- [24] O. Juillet and R. Frésard, *Phys. Rev B* **87**, 115136 (2013).
- [25] A. Leprévost, O. Juillet and R. Frésard, *Ann. Phys. (Berlin)* **526**, 430 (2014).
- [26] N. Tomita and S. Watanabe, *Phys. Rev. Lett.* **103**, 166401 (2009).
- [27] R. Rodríguez-Guzmán, C. Jiménez-Hoyos and G. Scuseria, *Phys. Rev. B* **90**, 195110 (2014).
- [28] See Supplemental Material at (URL to be inserted) for a comparison of the results originating from the symmetry projected HF/BdG wavefunction to existing data obtained by other numerical simulations.
- [29] Full periodic boundary conditions on our finite-size cluster could bias pairing correlations by disadvantaging the $d_{x^2-y^2}$ channel: The corresponding wavefunction in momentum space would indeed be zero for a non-negligible fraction of wavevectors in the first Brillouin zone.
- [30] The rapidly decaying one-particle contributions in Eq. (4) are discarded so that $\mathcal{D}(\vec{r})$ vanishes in the non-interacting limit. Precisely, the quantity

$\langle \hat{c}_{\vec{r}_1\sigma_1}^\dagger \hat{c}_{\vec{r}_4\sigma_4} \rangle_{\Psi_\Gamma} \langle \hat{c}_{\vec{r}_2\sigma_2}^\dagger \hat{c}_{\vec{r}_3\sigma_3} \rangle_{\Psi_\Gamma} - \langle \hat{c}_{\vec{r}_1\sigma_1}^\dagger \hat{c}_{\vec{r}_3\sigma_3} \rangle_{\Psi_\Gamma} \langle \hat{c}_{\vec{r}_2\sigma_2}^\dagger \hat{c}_{\vec{r}_4\sigma_4} \rangle_{\Psi_\Gamma}$ is subtracted for each term of the form $\langle \hat{c}_{\vec{r}_1\sigma_1}^\dagger \hat{c}_{\vec{r}_2\sigma_2}^\dagger \hat{c}_{\vec{r}_3\sigma_3} \hat{c}_{\vec{r}_4\sigma_4} \rangle_{\Psi_\Gamma}$.

- [31] P. Corboz, S. R. White, G. Vidal and M. Troyer, Phys. Rev. B **84**, 041108(R) (2011).
- [32] P. Corboz, T.M. Rice and M. Troyer, Phys. Rev. Lett. **113**, 046402 (2014).
- [33] M. Dierzawa and R. Frésard, Z. Phys. B **91**, 245 (1993).
- [34] R. Peters and N. Kawakami, Phys. Rev. B **89**, 155134 (2014).
- [35] C.-C. Chang and S. Zhang, Phys. Rev. Lett. **104**, 116402 (2010).
- [36] D. Bormann, T. Schneider and M. Frick, Europhys. Lett. **14**, 101 (1991).

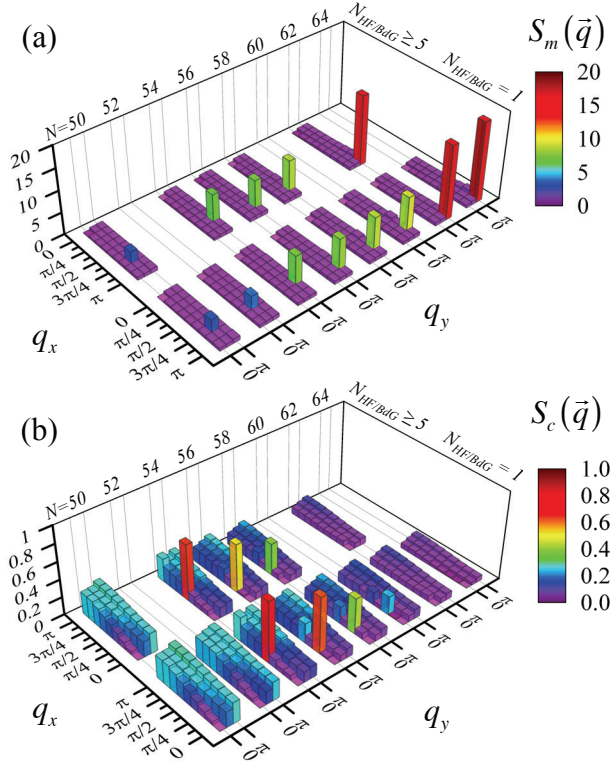


Fig. 1 (color online). Momentum dependence of (a) magnetic and (b) charge structure factors for hole dopings $\delta < 1/4$ at large interaction strength $U/t = 12$. A rectangular 16×4 cell is considered. Spin and density autocorrelation functions are calculated from the numerical solution of the symmetry projected HF/BdG scheme. All symmetries are restored through projections on the number of atoms N , a zero total pseudo-momentum \vec{K} , the spin-singlet subspace and the irreducible representation A_1 of the C_{2v} lattice symmetry group. The latter is physically associated to a many-body wavefunction invariant under horizontal and vertical mirrors. Note that these quantum number projections are also included during the energy minimization, except for the total spin where only its z -component and parity are imposed. In both parts (a) and (b), 3D-histograms in the front are obtained with one HF/BdG pair of states, while those in the back result from an enlarged subspace spanned by several sequentially optimized HF/BdG wavefunctions (five couples for $N = 50, 54, 58, 62$ and ten couples for $N = 56$). Both correlation functions show little sensitivity to the improvement of the variational state.

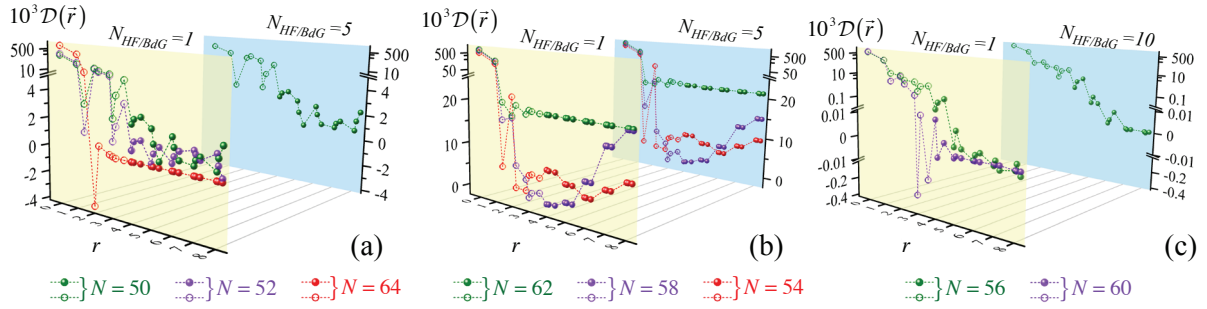


Fig. 2 (color). Dependence of the d -wave pair correlation function $\mathcal{D}(\vec{r})$ against separation distance r for different numbers N of atoms at strong coupling $U/t = 12$. In (b), note the oscillations at $r > 4$ in the stripe-like states with a full charge period λ_c for $N = 54$ and half a period for $N = 58$. The same wavefunctions as for Fig. 1 are used. Short and long-ranged parts of $\mathcal{D}(\vec{r})$ are indicated by open and full symbols, respectively. They are not affected by the improvement of the variational ansatz, as shown in the back of parts (a), (b) and (c).

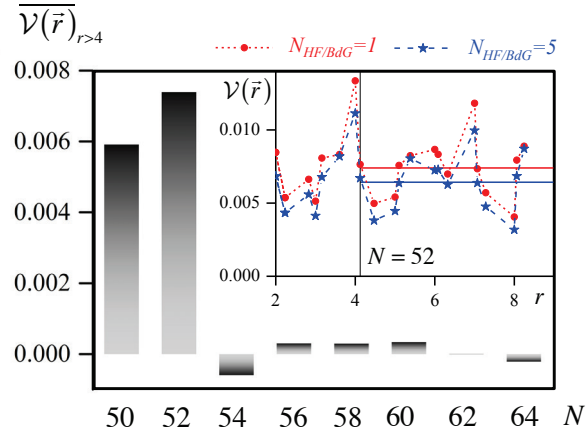


Fig. 3 (color online). Spiral correlation function $\mathcal{V}(\vec{r})$ averaged over large distances $r > 4$ against the lattice filling for $U/t = 12$. The same wavefunctions as for Fig. 1 are used. However, performing the full spin projection for such a four-body observable is beyond reach. We limit ourselves here to impose the z -component S_z and the spin-parity in addition to the restoration of all other symmetries. The detailed behavior of $\mathcal{V}(\vec{r})$ is shown in the inset for $N = 52$ atoms. Note the small difference between full circles and stars that correspond to one and five HF/BdG pair(s) of states, respectively.

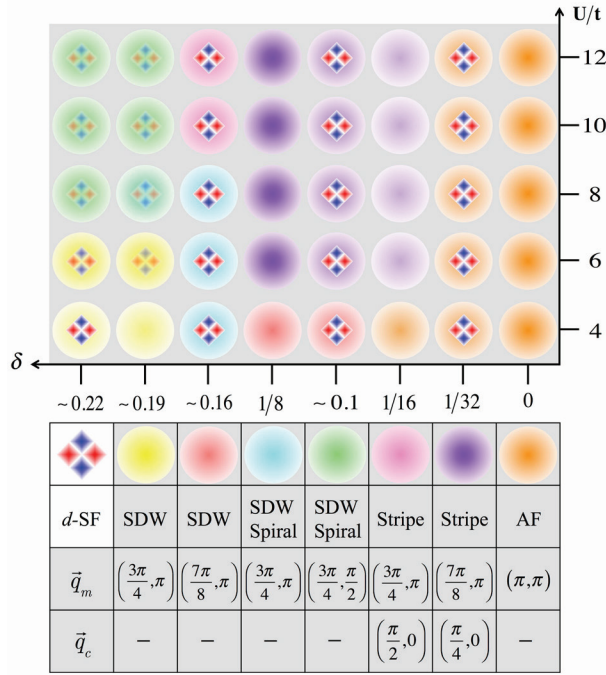


Fig. 4 (color). Phase diagram arising from the symmetry projected HF/BdG approach for 2D cold fermions described by the repulsive Hubbard model. Colors refer to different magnetic (charge) orders revealed by a peak at the wavevector \vec{q}_m (\vec{q}_c) in the Fourier transform of the spin (density) autocorrelation function. For each hole doping δ and interaction strength U/t , the d -wave superfluidity symbol is made more visible when the pair correlation function exhibits off-diagonal long-ranged order.

Supplemental Material for “Intertwined orders of ultracold fermions loaded in two-dimensional optical lattices”

A. Leprévost¹, O. Juillet¹ and R. Frésard²

¹ *Laboratoire LPC Caen, ENSICAEN, Université de Caen, CNRS/IN2P3, Caen, France.*

² *Laboratoire CRISMAT, UMR CNRS-ENSICAEN 6508, Caen, France.*

We present here the key features of the unbiased method used in the main text to approximate the ground-state of the two-dimensional Hubbard model, together with several numerical tests of the approach. We first focus on the variational equations for a trial state $|\Psi_\Gamma\rangle$ defined as the superposition of unrestricted Hartree-Fock (HF) and Bogoliubov-de Gennes (BdG) wavefunctions with symmetry projection before variation:

$$|\Psi_\Gamma\rangle = \hat{P}_\Gamma \left(x^{(HF)} |\Phi^{(HF)}\rangle + x^{(BdG)} |\Phi^{(BdG)}\rangle \right) \quad (1)$$

The restoration of quantum numbers Γ is ensured by the Peierls-Yoccoz [1] operator \hat{P}_Γ , which reads as a specific linear combination of symmetry transformations \hat{U}_g : $\hat{P}_\Gamma = \sum_g \lambda_{\Gamma,g} \hat{U}_g$.

The coefficients $\lambda_{\Gamma,g}$ are proportional to the characters of the irreducible representation associated to Γ . Noting that the transformed vectors $|\Phi_g^{(a)}\rangle = \hat{U}_g |\Phi^{(a)}\rangle$ (with the label a specifying the HF or BdG part) remain mean-field states, the projected energy $E_\Gamma = \langle \hat{H} \rangle_{\Psi_\Gamma}$ can be further calculated according to:

$$E_\Gamma = \frac{\sum_{a,b \in \{HF, BdG\}} x^{(a)*} x^{(b)} \sum_g \lambda_{\Gamma,g} \mathcal{N}_g^{(a,b)} \mathcal{E}[\mathcal{R}_g^{(a,b)}]}{\sum_{a,b \in \{HF, BdG\}} x^{(a)*} x^{(b)} \sum_g \lambda_{\Gamma,g} \mathcal{N}_g^{(a,b)}} \quad (2)$$

\mathcal{E} stands for the energy functional obtained with Wick’s theorem. However, the normal contractions $\langle \hat{c}_{\vec{r}\sigma}^\dagger \hat{c}_{\vec{r}'\sigma'} \rangle$, $\langle \hat{c}_{\vec{r}\sigma} \hat{c}_{\vec{r}'\sigma'}^\dagger \rangle$ now correspond to matrix elements between the non-orthogonal wavefunctions $|\Phi^{(a)}\rangle$ and $|\Phi^{(b)}\rangle$, divided by their overlap $\mathcal{N}_g^{(a,b)}$ [2,3]. They define the one-body (transition) density matrix elements $[\rho_g^{(a,b)}]_{\vec{r}'\sigma', \vec{r}\sigma}$, $[\tilde{\rho}_g^{(a,b)}]_{\vec{r}'\sigma', \vec{r}\sigma}$. Similar features apply to the anomalous contributions $\langle \hat{c}_{\vec{r}\sigma} \hat{c}_{\vec{r}'\sigma'} \rangle$, $\langle \hat{c}_{\vec{r}\sigma}^\dagger \hat{c}_{\vec{r}'\sigma'}^\dagger \rangle$ that identify to the pairing tensors elements $[\kappa_g^{(a,b)}]_{\vec{r}'\sigma', \vec{r}\sigma}$, $[\tilde{\kappa}_g^{(a,b)}]_{\vec{r}'\sigma', \vec{r}\sigma}$. Both types of contractions are gathered in the

extended matrix $\mathcal{R}_g^{(a,b)} = \begin{pmatrix} \rho_g^{(a,b)} & \kappa_g^{(a,b)} \\ \tilde{\kappa}_g^{(a,b)} & \tilde{\rho}_g^{(a,b)} \end{pmatrix}$ that can be easily expressed in terms of

quasiparticle states, occupied and unoccupied HF wavefunctions [4]. Stationnarity of E_Γ Eq. (2) with respect to the amplitudes $x^{(HF)}$ and $x^{(BdG)}$ immediately leads to a generalized eigenvalue equation:

$$\sum_{b \in \{HF, BdG\}} x^{(b)} \sum_g \lambda_{\Gamma, g} \mathcal{N}_g^{(a,b)} \left(\mathcal{E}[\mathcal{R}_g^{(a,b)}] - E_\Gamma \right) = 0 \quad (3)$$

By contrast, the energy minimization with respect to the spin-orbitals $\phi_{i, \bar{r}\sigma}$ and Bogoliubov coefficients $U_{\bar{r}'\sigma', \bar{r}\sigma}$, $V_{\bar{r}'\sigma', \bar{r}\sigma}$ is much more involved and will be detailed in a forthcoming paper [4]. It leads to a self-consistent equation that reads:

$$\sum_{b \in \{HF, BdG\}} x^{(b)} \mathcal{L}_\Gamma^{(a,b)} = 0 \quad (4)$$

where the matrices $\mathcal{L}_\Gamma^{(a,b)}$ are obtained with the help of the HF/BdG mean-field Hamiltonian

$\mathcal{H}_{ij}[\mathcal{R}] = \frac{1}{2} \frac{\partial \mathcal{E}[\mathcal{R}]}{\partial \mathcal{R}_{ji}}$ as:

$$\mathcal{L}_\Gamma^{(a,b)} = \sum_g \lambda_{\Gamma, g} \mathcal{N}_g^{(a,b)} \left[\left(1 - \mathcal{R}_g^{(a,b)} \right) \mathcal{H}[\mathcal{R}_g^{(a,b)}] \mathcal{R}_g^{(a,b)} + \mathcal{R}_g^{(a,b)} \left(\mathcal{E}[\mathcal{R}_g^{(a,b)}] - E^{(\Gamma)} \right) \right] \quad (5)$$

One the most attractive features of the scheme Eqs. (3)-(5) relies on its ability to reveal the physics spontaneously emerging from the Hubbard Hamiltonian through a numerical solution in which the HF and BdG states are parameterized according to the Thouless theorem [2]. For weak coupling strength U/t , such an unbiased determination of the favored correlations can also be achieved by identifying the channels in which instabilities develop through self-consistent perturbative or functional renormalization group methods [5,6]. In the strongly correlated regime, the problem could ideally be tackled with Gutzwiller-type wavefunctions $|\Psi_g\rangle = \hat{P}_G |\Phi\rangle$ where the operator $\hat{P}_G = \prod_{\bar{r}} (\hat{1} - g \hat{n}_{\bar{r}\uparrow} \hat{n}_{\bar{r}\downarrow})$ partially suppresses the double occupancy entailed in a mean-field state $|\Phi\rangle$ through the real parameter g [7]. Yet, the energy minimization has to be performed in a variational Monte-Carlo framework, rendering unrestricted calculations beyond reach. Hence, the reference wavefunction must be parameterized with a limited number of relevant variables to describe specific phases, such as d -wave superfluids [8], spirals [9] or stripes [10]. A step towards unbiased Gutzwiller calculations has been recently achieved [11]. However, orders exhibiting a periodicity larger than a few lattice spacings were forbidden, in contradiction to approximate QMC results revealing long wavelength modes in ground-states.

We now address the reliability of the symmetry projected HF/BdG scheme against exact diagonalization (ED) for small clusters or quantum Monte-Carlo (QMC) simulations. First we focus on the spin, charge and d -wave pair correlation functions considered in the main text [12]. For a 4×4 cluster in the strong coupling regime $U/t = 10, 12$, the HF/BdG approximation reproduces very accurately the ED data, as shown in Figs. 1-2. The determination of exact ground states for larger cells is still limited by the NP-hardness of QMC simulations, except for limited parameter spaces where the stochastic sampling is protected from the notorious sign problem. This is the case at half-filling and we present in Fig. 3 a comparison between QMC and HF/BdG spin-spin correlations for a 6×6 cluster at $U/t = 4$. No significant difference is found, especially for the largest separation distances that are essential to indicate the development of a magnetic order. In the hole doped regime with repulsive interactions, a sign-free stochastic sampling of the ground-state is certainly possible [13,14], but it remains generally plagued by systematic errors which origin is not totally elucidated [15]. Nevertheless, it seems that these new QMC algorithms can be accurate for closed-shell fillings and moderate interaction strengths when supplemented by quantum number projections [15,16]. Superfluid correlations in the d -wave channel have been investigated in such a framework [17] and we show in Fig. 4a a representative result from

Ref. [11] in the intermediate coupling regime $U/t = 4$ on a 8×8 cell. The symmetry-adapted HF/BdG wavefunction essentially yields the same pairing response $\mathcal{D}(\vec{r})$, as shown in Fig. 4b.

Besides, the variational energies E_Γ originating from Eqs. (3)-(5) are summarized in Table 1 for the clusters and on-site interactions previously considered. The agreement is excellent for 4×4 cells with a relative error smaller than 0.5%. The quality of the approximation is quite similar for their doped counterparts, even when a negative next-nearest neighbor hopping t' is introduced to induce frustration. As the size increases, the HF/BdG energy becomes generally less accurate and the deterioration is more pronounced if the cell is doped and/or the coupling U/t is strong. Indeed, while the discrepancy for the half-filled 6×6 cluster at $U/t = 4$ does not exceed 0.5%, for 64-sites cells and up to $U/t \sim 12$, we only recover an energy E_Γ very close to the one obtained with the optimized BCS-Gutzwiller wavefunction [8].

For the largest clusters, the above contradictory findings, regarding the accuracy of HF/BdG correlation functions and energies, could be reconciled provided that improving the ansatz Eq. (1) noticeably affects the energy only. This scenario has been validated by enlarging the variational subspace through the inclusion of several HF/BdG pairs of states.

Thus, the ansatz Eq. (1) becomes $|\Psi_\Gamma\rangle = \hat{P}_\Gamma \left(\sum_{i=1}^{N_{\text{HF/BdG}}} \sum_{a_i \in \{\text{HF, BdG}\}} x^{(a_i)} |\Phi^{(a_i)}\rangle \right)$ and the full energy

minimization would then require the simultaneous variation of all HF and BdG states. This scheme is beyond our computational facilities and we therefore limit ourselves to a sequential process. In this case, HF/BdG pairs are progressively introduced and each of them is optimized while keeping unchanged the previous basis states. The amplitudes $x^{(a_i)}$ are obtained through a generalized eigenvalue problem similar to Eq. (3) and the self-consistent equation determining the structure of the current HF/BdG pair now reads as

$$\sum_{j=1}^i \sum_{b_j \in \{\text{HF, BdG}\}} x^{(b_j)} \mathcal{L}_\Gamma^{(a_i, b_j)} = 0 \quad (6)$$

In the case of a doped 6×6 cell with $N = 24$ interacting atoms at $U/t = 8$, the symmetry adapted HF/BdG approximation with one pair of states leads to a variational energy $E_\Gamma = -34.93 t$. The use of 50 HF/BdG pairs allows to reach an energy of $-36.9 t$ which is comparable to approximate QMC estimates depending on the constraining state chosen to avoid the sign problem [18]. As shown in Fig. 5, such an improvement of the trial wavefunction Eq. (1) induces minimal changes in the spin, charge and d -wave pair correlation functions. A similar behavior has been reported in the main text for the 16×4 cluster.

Finally, the present calculations tend to support the HF/BdG approximation with full symmetry restoration before variation as a reliable starting point to capture the essence of correlations entailed in the Hubbard model, at least in the magnetic, density, and superfluid channels and for moderate size clusters.

- [1] M. Hamermesh, *Group Theory and its Applications to Physical Problems* (Addison-Wesley, Reading, MA, 1962).
- [2] J.-P. Blaizot and G. Ripka, *Quantum Theory of Finite Systems* (MIT Press, Cambridge, 1985).
- [3] The overlap $\mathcal{N}_g^{(a,b)} = \langle \Phi^{(a)} | \Phi_g^{(b)} \rangle$ is a determinant for two HF wavefunctions (see Ref. [2]) and a pfaffian otherwise (see G. F. Bertsch and L. M. Robledo, Phys. Rev. Lett. **108**, 042505 (2012)).
- [4] A. Leprévost, O. Juillet and R. Frésard, in preparation.
- [5] C. J. Halboth and W. Metzner, Phys. Rev. B **61**, 7364 (2000).
- [6] W. Metzner, M. Salmhofer, C. Honerkamp, V. Meden, and K. Schönhammer, Rev. Mod. Phys. **84**, 299 (2012).
- [7] D. Vollhardt, Rev. Mod. Phys. **56**, 99 (1984).
- [8] T. Giamarchi and C. Lhuillier, Phys. Rev. B **42**, 10641 (1990).
- [9] M. Dzierzawa and R. Frésard, Z. Phys. B **91**, 245 (1993).
- [10] M. Miyazaki, K. Yamaji, T. Yanagisawa and R. Kadono, J. Phys. Soc. Jpn **78**, 043706 (2009).
- [11] T. Misawa and M. Imada, Phys. Rev. B **90**, 115137 (2014).
- [12] All the HF/BdG calculations of the d -wave pairing correlation function $\mathcal{D}(\vec{r})$ presented in the Supplemental Material include the one-body contributions to compare with existing data.
- [13] J.F. Corney and P.D. Drummond, Phys. Rev. Lett **93**, 260401 (2004).
- [14] O. Juillet, New J. Phys. **9**, 163 (2007).
- [15] F.F. Assaad, P. Werner, P. Corboz, E. Gull and M. Troyer, Phys. Rev. B **72**, 22451 (2005).
- [16] T. Aimi and M. Imada, J. Phys. Soc. Jpn. **76**, 084709 (2007).
- [17] T. Aimi and M. Imada, J. Phys. Soc. Jpn. **76**, 113708 (2007).
- [18] H. Shi, C. A. Jimenez-Hoyos, R. Rodriguez-Guzman, G. Scuseria, and S. Zhang, Phys. Rev. B **89**, 125129 (2014).
- [19] B. Bauer, L. D. Carr, H. G. Evertz, A. Feiguin, J. Freire, S. Fuchs, L. Gamper, J. Gukelberger, E. Gull, S. Guertler, A. Hehn, R. Igarashi, S. V. Isakov, D. Koop, P. N. Ma, P. Mates, H. Matsuo, O. Parcollet, G. Pawłowski, J. D. Picon, L. Pollet, E. Santos, V. W. Scarola, U. Schollwöck, C. Silva, B. Surer, S. Todo, S. Trebst, M. Troyer, M. L. Wall, P. Werner and S. Wessel, J. Stat. Mech. **P05001** (2011).

Table I. Variational energies E_{Γ} from the symmetry projected HF/BdG wavefunction compared to reference energies $E_{ref.}$ obtained either with exact diagonalization (ED), quantum Monte-Carlo (QMC) or variational Monte-Carlo (VMC) results. Periodic-periodic (PP) or periodic-antiperiodic (PA) boundary conditions are specified. The symbol (*) indicates a simulation of the frustrated Hubbard model with an hopping amplitude $t' = -0.3t$ between next-nearest neighbors. Exact diagonalization has been performed with ALPS [19]. QMC data are borrowed from Ref. [10,14]. The VMC calculation corresponds to the BCS-Gutzwiller wavefunction of Ref. [8].

Lattice	U/t	Boundary	N	E_{Γ}/t	$E_{ref.}/t$
4×4	4	PP	16	-13.618	-13.622 (ED)
4×4 (*)	8	PP	14	-12.439	-12.503 (ED)
4×4	10	PP	10	-16.876	-16.902 (ED)
4×4	12	PP	14	-9.957	-10.05 (ED)
6×6	4	PP	36	-30.724	-30.87(2) (QMC)
8×8	4	PP	50	-70.13	-72.51(5) (QMC)
8×8	10	PA	60	-32.164	-31.2 (VMC)

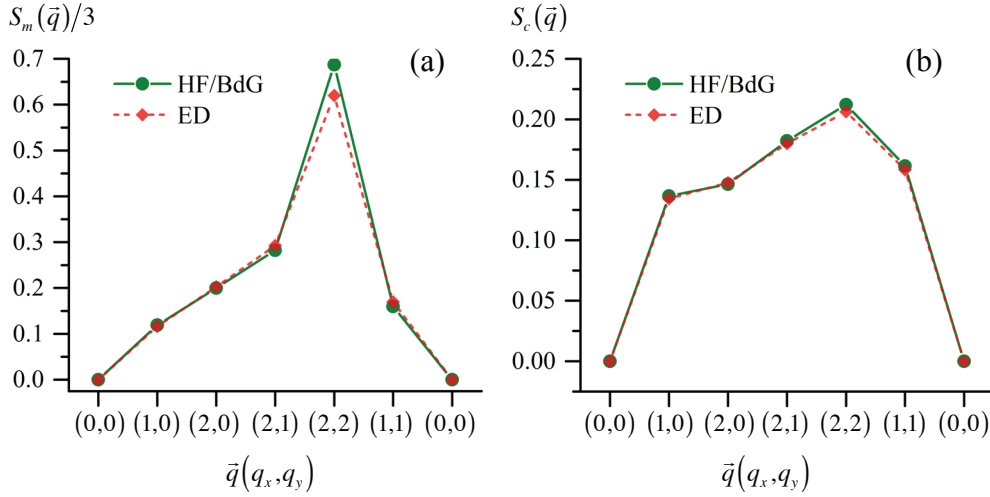


Fig. 1. Momentum dependence of (a) magnetic $S_m(\vec{q})$ and (b) charge $S_c(\vec{q})$ structure factors for a 4×4 cluster with $N=14$ atoms and periodic-periodic boundary conditions in the strongly correlated regime $U/t=12$. Wavevectors \vec{q} are expressed in units of $\pi/2$. A symmetry projected HF/BdG pair of states displays excellent agreement with exact diagonalization.

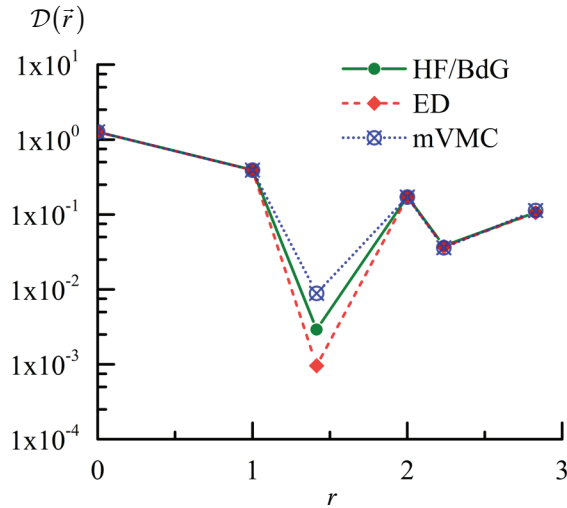


Fig. 2. d -wave pair correlation function $\mathcal{D}(\vec{r})$ against separation distance r for a 4×4 lattice with $N=10$ atoms at strong on-site interaction $U/t=10$. Periodic-periodic boundary conditions are imposed. ED results as well as a recent VMC calculation with a symmetry restored BCS-Gutzwiller wavefunction (mVMC) are extracted from Fig. 8b of Ref. [11]. The HF/BdG ansatz, with quantum number projections before variation, correctly reproduces the shape and magnitude of the exact pairing correlations.

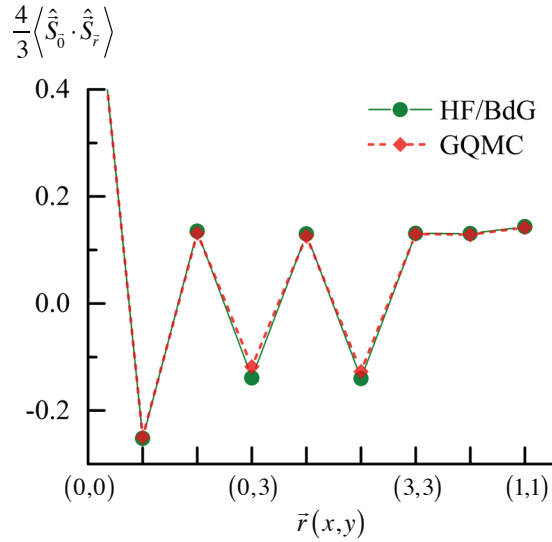


Fig. 3. Spin-spin correlations $\langle \hat{S}_0 \cdot \hat{S}_{\vec{r}} \rangle$ at half-filling for a periodic-periodic 6×6 cluster at $U/t = 4$ as obtained from the symmetry restored HF/BdG approach and compared with QMC calculations incorporating quantum number projections (GQMC, extracted from Fig. 2 of Ref. [15]).

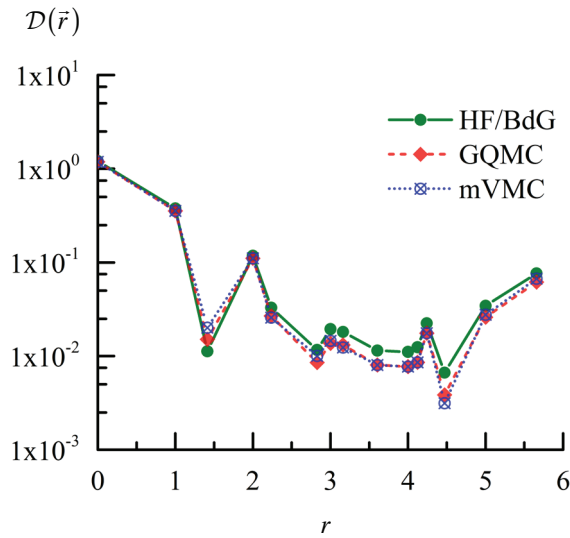


Fig. 4. Distance dependence of the d -wave pair correlation function $\mathcal{D}(\vec{r})$ for a 8×8 cell with $N = 50$ atoms and periodic-periodic boundary conditions at moderate coupling strength $U/t = 4$. Sign-free QMC calculations (GQMC) and VMC results with the BCS-Gutzwiller wavefunction (mVMC), both including symmetry restoration, are extracted from Fig. 10 of Ref. [11]. They are compared to the pairing correlations $\mathcal{D}(\vec{r})$ originating from the symmetry adapted HF/BdG scheme.

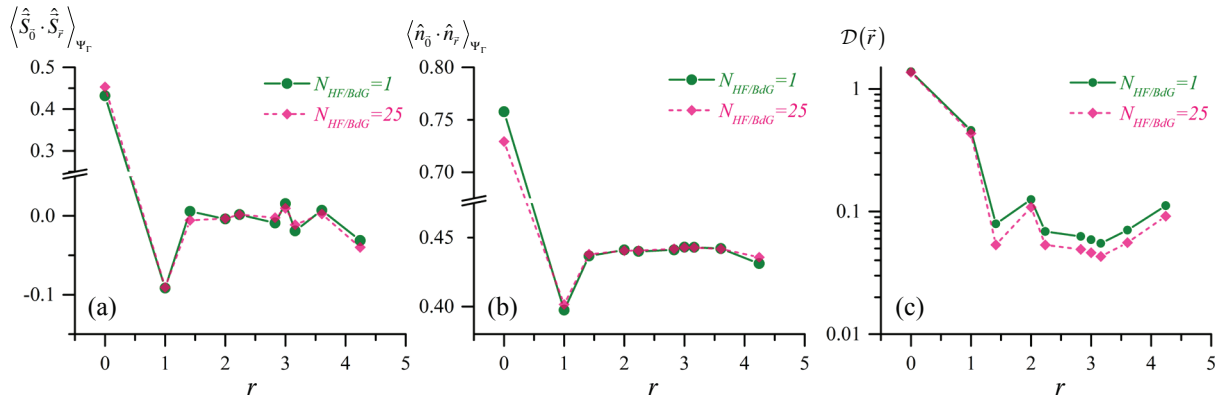


Fig. 5. Evolution of (a) spin, (b) density and (c) d -wave pairing autocorrelation functions with the number $N_{\text{HF/BdG}}$ of symmetry projected HF/BdG wavefunctions spanning the variational subspace. Calculations are performed for $N = 24$ atoms on a 6×6 cluster with an interaction strength $U/t = 8$.